INTERNATIONAL JOURNAL OF AUTOMOTIVE AND MECHANICAL ENGINEERING
ISSN: 2229-8649 e-ISSN: 2180-1606
VOLUME 22, ISSUE 2, 2025, 12388 - 12403
DOI: https://doi.org/10.15282/ijame.22.2.2025.11.0948

RESEARCH ARTICLE

Experimental Analysis of Thermodynamic Performance for 2.5 kW Split Inverter Air Conditioning Unit with R-410A

I Gede Artha Negara*, I Wayan Temaja, Luh Putu Ike Midiani, I Dewa Made Cipta Santosa, I Gusti Agung Bagus Wirajati, Made Ery Arsana

Department of Mechanical Engineering, Bali State Polytechnic, 80364 Badung, Indonesia

ABSTRACT – This research aims to investigate the thermodynamic performance, including temperature differential properties and energy efficiency ratio (EER) of the air conditioning cooling system. A 2.5 kW split inverter air conditioning system with R-410A refrigerant was used in this research for investigation and integrated with an ATmega 2560 microcontroller for data acquisition. The investigation was carried out between the temperature setpoints of 16°C and 20°C. An online psychrometric chart calculator was employed in this research to facilitate the calculation of thermodynamic properties. The results showed that the average temperature differential across all the temperature setpoints was found to be 11°C to 12.89°C. This result indicated an ability to exceed the minimum tolerance allowed for evaporator temperature differential standards. Moreover, the highest result of the EER of the air conditioning system was 13.87 at a temperature setpoint of 20°C. The research revealed that all temperature setpoints ranging from 16°C to 20°C yielded EER values within the range of 8 to 15, which is widely recognized as the efficient operational range for residential air conditioning applications. In addition, this air conditioning system has better energy efficiency and cost savings over the lifetime of the cooling system. The integration of microcontroller technology in this research facilitated the real-time recording of each investigation parameter. This approach enhanced the efficiency, complexity, and reliability of the experimental investigation of the air conditioning system.

ARTICLE HISTORY

Received	:	28th May 2024
Revised	:	14th Feb. 2025
Accepted	:	06th May 2025
Published	:	12th June 2025

KEYWORDS

Energy efficiency ratio
Temperature differential
Inverter air conditioning
Thermodynamic

1. INTRODUCTION

Air conditioning is a trustworthy device that increases human comfort in a compartment or for residential purposes. Lately, the demand for air conditioning installations has increased significantly, resulting in an increase in electrical energy consumption [1]–[5]. Unfortunately, this phenomenon has a negative effect on electrical energy consumption over time. Based on the report [6], one of the biggest contributors to energy consumption in appliances is air conditioning, including houses, industrial plants and property. According to the report, roughly 15% of world electrical energy consumption comes from refrigeration and air conditioning systems [7]. However, energy consumption in air conditioning is found to be around 20% in developing countries such as Indonesia [6]. The most familiar unit for air conditioning is vapor-compression refrigeration. This device is widely used for refrigerators, air conditioners, and heat pumps [8], [9]. The main components of the unit are the evaporator, compressor, condenser and expansion valve [10]–[12]. This unit comprises four processes: 1-2: Compression in isentropic compressor. The next process is 2-3: Heat removal in a condenser with isobar. 3-4: Expansion of throttling. 4-1: Thermal absorption in an evaporator with isobar. All components related to vapor-compression refrigeration are steady-flow. As a result, all processes can be investigated as steady-flow processes [13]–[16].

In the field of air conditioning technology, the use of inverter technology represents a groundbreaking advancement aimed at addressing the issue of electrical energy consumption [17], [18]. The operational mechanism of an inverter-based air conditioning system differs slightly from that of conventional air conditioning systems. The inverter is able to control the compressor rotation speed, thereby reducing the binary on/off cycle [19]. The inverter can regulate the flow rate of refrigerant by evolving the compressor speed [20], [21]. On the other hand, conventional air conditioning is generally operated at a fixed speed. The advantages of inverter air conditioning include the ability to save more energy, enhance temperature regulation, and extend longevity [22], [23]. Moreover, inverter air conditioning systems typically generate less noise compared to traditional air conditioning units. In order to determine the efficiency of an air conditioning cooling system, a thermodynamic parameter is required, known as the energy efficiency ratio (EER). The EER is a measure that compares the rate of heat removal from the cooled space to the rate of energy consumption by the air conditioning system [24]. The higher EER indicates the higher energy efficiency of the air conditioning system. Globally, the range of EER for current residential air conditioning systems is typically around 8-12 [25]. However, for commercial air conditioning systems, the range of EER can be around 10-16 or even higher. In addition, the EER is

***CORRESPONDING AUTHOR | I. Gede Artha Negara** | ✉ artha_negara@pnb.ac.id

commonly utilized as a metric to rate the efficiency of air conditioning systems under specific operating conditions, including indoor and outdoor temperatures, as well as relative humidity levels [26].

In a previous study, Watcharajinda et al. [27] investigated the effectiveness of an open pond as a heat sink for a water-cooled condenser rather than a cooling tower. A 3.5 kW air conditioner using R32 and an open pond was utilized in the study. The research shows the capability of employing an open pond as a heat sink, leveraging evaporative and heat exchanger mechanisms. This research aims to sustain the air conditioner energy efficiency ratio (EER) beyond 4.1 by modifying the surface area as well as the pond volume ratio. In the research, the air-conditioned chamber temperature was sustained at 23°C and a 4 kW electrical heater was applied as thermostatic control. In the next study, Andrade et al. [6] conducted an examination of fixed types of air conditioning equipment under various thermal load states using a method of EER and cooling seasonal performance factor (Fcsp). Research shows detailed revision procedures, standard states, and a comparison of the results between the two types of air conditioning. This result indicated that the EER method was found to be more accurate when assessed by the Fcsp under real operating conditions. This result could be beneficial for improving public policies and advanced technical planning for developing and designing energy efficiency applications. A study from Conte et al. [24] conducted an experimental study on the use of low GWP refrigerants as drop alternatives to refrigerant R134a in a compression system with water-to-water vapor. The types of refrigerants employed for investigation are: R513A, R450A, R515B, R516A, R152a, and R1234ze(E). The experimental tests were conducted at full and partial loads with a fixed outlet/inlet temperature of water in the heat exchanger. The experimental data allowed for the analysis of the energy efficiency ratio (EER) for each type of refrigerant respectively. The data compare each refrigerant of R134a: R450A and R152a, which can reach up to 3.8% and 8.5% higher EER, respectively.

This research study investigated the thermodynamic performance, specifically the energy efficiency ratio (EER) of a split wall inverter air conditioning unit. The experiments were conducted under standardized room heat load conditions. The study utilizes microcontroller technology to log data for each of the investigated parameters. The role of the microcontroller was to provide accurate and precise real-time data. The tests were carried out with varying air conditioning temperature setpoints. This allowed for a comprehensive analysis of the system's energy efficiency characteristics under different operational conditions. The primary objective of this research study is to evaluate the thermodynamic performance, specifically the EER of inverter air conditioning cooling systems under actual operating conditions. Furthermore, this investigation aims to provide comprehensive innovations in microcontroller technology-based instrumentation for data acquisition and analysis. In addition to the EER assessment, this study also examines the range of temperature differential between the evaporator inlet and outlet. This parameter provides valuable insights into the heat transfer characteristics and efficiency of the refrigeration cycle within the air conditioning system. The findings from this study will contribute to a deeper understanding of the energy efficiency characteristics of a split wall inverter air conditioning unit under actual operating conditions.

2. EXPERIMENTAL AND INSTRUMENTATION SETUP

This research was conducted in the Air Conditioning and Refrigeration Laboratory, Mechanical Engineering Department at Bali State Polytechnic. The air conditioning used in this study was a 2.5 kW split-type inverter air conditioner utilizing R-410A as the working refrigerant. The specific system specifications can be seen in Table 1. This air conditioning is provided with inverter technology, which is able to control the compressor speed and minimize on/off cycles. This research investigation employed an ATmega 2560 microcontroller as the data logging system. This microcontroller-based setup was utilized to record various system parameters and also provide a real-time display of the monitored data. The ATmega 2560 has pins for 54 digital input/output [28], [29] 16 analog inputs and operates at 16 MHz. The technical details of the ATmega 2560 are shown in Table 2 [30]. The experimental setup utilized the latest version of the Arduino integrated development environment (IDE) software installed on a personal computer to program the ATmega 2560 microcontroller. The Arduino IDE provided a user-friendly platform for the development and implementation of the custom firmware required to operate the data logging and monitoring system based on the ATmega 2560 microcontroller [31]. The k-type thermocouple was applied in this research to measure the temperature of the inlet and outlet evaporator. This k-type thermocouple has a measurement range from 0°C to 400°C with a specific error of ±2°C. In order to ensure the reliability and precision of the temperature measurements, the thermocouples were calibrated against a precision reference thermometer with an uncertainty of ±0.04°C. This calibration process was conducted to minimize any systematic errors and improve the overall accuracy of the temperature data collected during the experiments.

To measure relative humidity at the evaporator inlet and outlet, the DHT22 sensor was used in this study with a measurement range of 0% to 100%. Moreover, the PZEM 004-T sensor was utilized in this research to quantify electrical parameters, including voltage, current and power consumption. The integration of these specialized sensors into the experimental setup allowed for the simultaneous monitoring of the thermodynamic, psychrometric, and electrical parameters. All instrument accuracies were recorded in Table 3. A digital anemometer was utilized in this research to measure the wind speed of air conditioning. An 830-point breadboard was used to connect all electrical components. In order to save the data parameters of an SD card module employed in the installation via jumper cables. A schematic of the experimental setup can be seen in Figure 1. Additionally, online psychrometric diagrams were applied in this research to obtain thermodynamic properties, including enthalpy, dry bulb temperature, wet bulb temperature, relative humidity and specific volume. These psychrometric diagrams are crucial for determining the thermophysical properties of moist air, which is essential for the comprehensive analysis of the air conditioning system's performance. The psychrometric diagram software used was the online interactive psychrometric chart, which was established by FlyCarpet Inc. The ability to seamlessly integrate the psychrometric diagram software into the experimental analysis allowed for the accurate determination of the air properties at various points within the air conditioning system.

Table 1. Detailed specification of split inverter air conditioning unit

Model	Refrigerant: R-410A	
	Unit	Values
Cooling		
Input power	kW	0.485
Rated current	A	2.7
Maximum power	kW	2.06
Maximum current	A	9.5
Compressor speed range	RPM	600–3600
Capacity	kW	2.5
Heating		
Input power	kW	0.58
Rated current	A	3
Maximum power	kW	2.06
Maximum current	A	9.5
Compressor speed range	RPM	600–3600
Capacity	kW	3.2

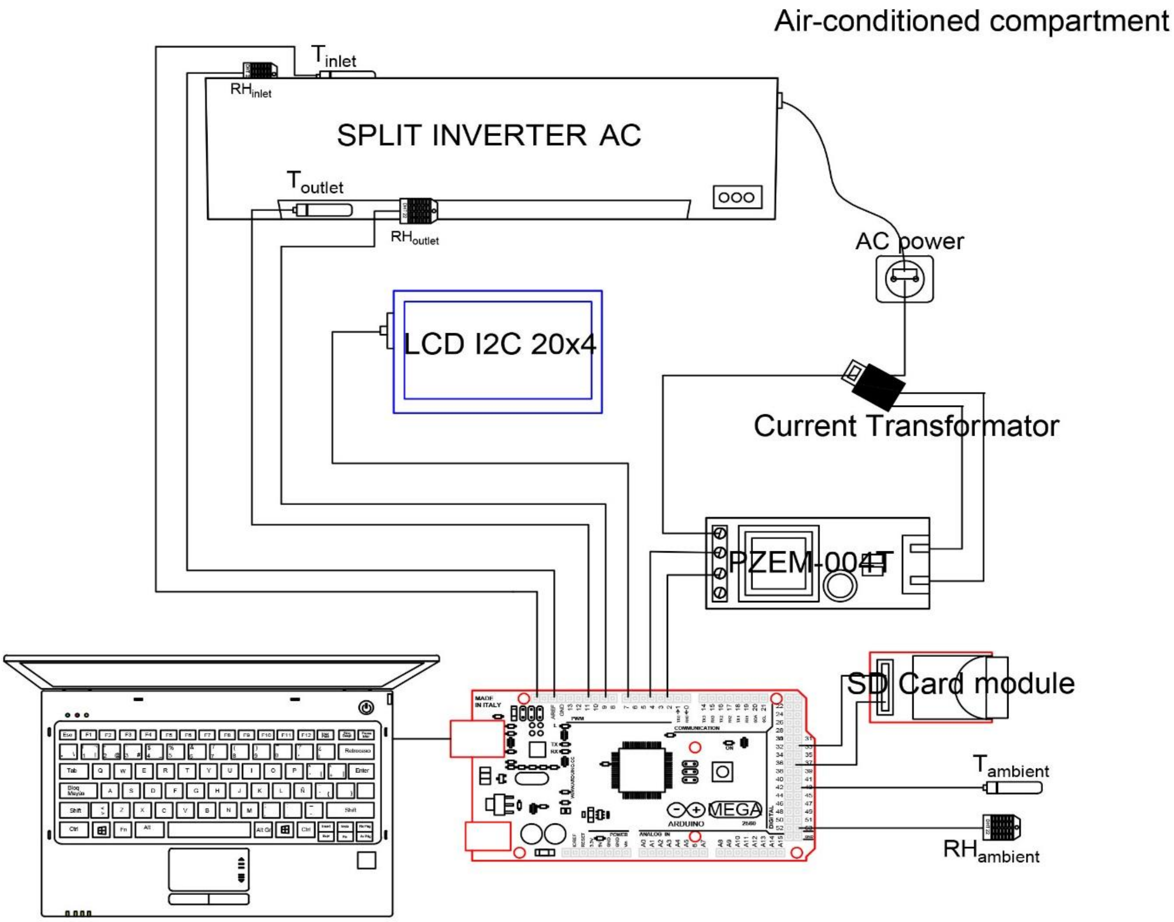

Figure 1. Schematic illustration of the experimental setup

Table 2. Detailed specification of microcontroller unit

Specification	Details
Microcontroller	ATmega 2560
Voltage of input	7V - 12V
Voltage of operating	5V
Pins of analog input	16
DC current per I/O pin	20 mA
Pins of digital I/O	54
DC current for 3.3V pin	50 mA
Clock speed	16 MHz
EEPROM	4 KB
Flash memory	256 KB (8 KB used by bootloader)
SRAM	8 KB
Communication interfaces	UART (4), I2C, SPI
PWM pins	15 (Pins: 2 to 13, 44 to 46)
USB connection	Type B USB port
ICSP header	Yes
Power jack	Yes
Onboard LED	Yes
Reset button	Yes
Weight	37 grams
Dimensions	101.52 mm x 53.3 mm

Table 3. Instruments accuracy

Parameter	Instrument	Range and unit	Accuracy
Temperature	K-type thermocouple Max6675	0°−400°C	±2°C
Relative humidity	DHT22	0%−100%	±2−5%
Wind speed	Anemometer	0.4−30 m/s	±3.5%
Power	PZEM-004T	0−10 kW	±3%
Current	PZEM-004T	0−100 A	±2%
Voltage	PZEM-004T	80−260 VAC	±1%

Figure 1 shows both thermocouple and DHT22 sensors positioned on the supply and inlet sides of the evaporators, respectively. These sensors are also placed in an air-conditioned compartment to measure the surrounding ambient air temperature and relative humidity levels. The dry-bulb temperature and relative humidity are utilized to determine thermodynamic properties such as enthalpy, humidity ratio and specific volume through psychrometric diagrams. The PZEM current transformer is connected to the air conditioning system's power to report electrical parameters. The I2C LCD is connected to the ATmega 2560 via jumper cable to serve as a display during the investigation. Furthermore, an SD card module equipped with memory is linked to the ATmega 2560 for data storage. All instrumentation components are connected to the ATmega 2560 microcontroller and integrated with a PC to receive commands in the coding format across the Arduino IDE application. The investigation was carried out over a duration of two hours, during which the temperature was varied across five distinct setpoints: A (16°C), B (17°C), C (18°C), D (19°C), and E (20°C). In addition, each parameter investigated is plotted on an online psychrometric chart to evaluate the thermodynamic properties of each temperature setpoint variation. This property is used to calculate the energy efficiency ratio (EER) for a 2.5 kW split inverter air conditioning system. The energy efficiency ratio (EER) is a metric that quantifies the performance and cooling efficiency of an air conditioning system. A higher EER value indicates a more energy-efficient AC system. In order to determine the EER value, several equations are required, including volume flow rate ($\dot{v}$) and mass flow rate ($\dot{m}$) as follows:

$$\dot{V} = V \times A \tag{1}$$

where V represents the airflow velocity through the evaporator fan (m/s), A is the cross-sectional area of the evaporator fan (m^2),

$$\dot{m} = \frac{\dot{v}}{v} \tag{2}$$

where $\dot{V}$ is the volumetric air flow rate (m^3/s), and V is the specific volume of air (m^3/kg). The cooling capacity can be determined by

$$Q_{out} = \dot{m} \times (h_{in} - h_c) \quad (3)$$

where $\dot{m}$ is the mass flow rate of the air (kg/s), h_{in} is the enthalpy of the inlet air (kJ/kg), and h_c is the enthalpy of the conditioned (cooled) air (kJ/kg). The energy efficiency ratio (EER) can be determined by

$$EER = \frac{Q_{out}}{P} \quad (4)$$

where Q_{out} is the heat removal rate from the cooled space (kW). P is the energy consumption rate by the air conditioning system (W).

3. RESULTS AND DISCUSSION

3.1 Evaporator Temperature

The variations in the outlet-side evaporator temperature from each temperature setpoint are shown in Figure 2. From the figure, it can be seen that all temperature setpoints decrease sharply to 25.75°C at approximately 1500s. Thereafter, the temperatures tend to continue decreasing as they approach 18°C. The TA temperature was observed to be relatively lower compared to the temperature setpoint. This is due to the TA indicating a temperature of 16°C, causing the compressor to work harder and operate for a longer duration to achieve the desired cooling effect. The lowest temperature on TA was found to be 12.5°C at around 6540s, after which slight fluctuations were observed due to variations in the room thermal load. The results indicate that lower temperature setpoints lead to correspondingly lower temperatures being achieved within the conditioned space [32]. Furthermore, the temperature measured at the TB was observed to be slightly similar to the TA. The difference in the temperatures recorded by TA and TB was inclined around 1°C. The temperatures indicated by the TC and TD were found to be slightly lower than those of TA and TB. However, based on the investigation, both TC and TD showed similar trends, as shown in Figure 2. The TC and TD were 17°C at 770s and relatively the same during the investigation. In addition, TE was observed to be higher than all temperature setpoints. This is because the compressor operated at a slower pace, resulting in a slightly higher temperature at the TE than the other measurement point [33], [34]. Generally, the outlet-side evaporator temperature shows low values across all the setpoint temperatures.

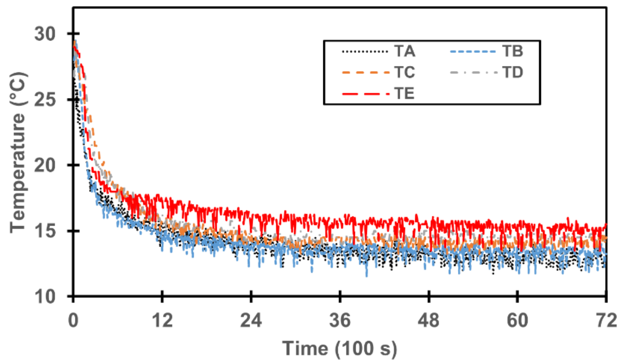

Figure 2. Temperature variation at the evaporator outlet correlated with temperature setpoint

Figure 3 shows the temperature variation in the inlet side of the evaporator across different temperature setpoints. From the observation, the temperature TA can be observed to decrease to 26°C around 1500s and exhibit fluctuations, likely due to the variable room heat load. The fluctuations observed in the inlet temperature are caused by an unstable and changing heat load within the room. The behavior is the entry and exit of occupants into the room, which would result in transient changes in the room's thermal load. This effect introduces disturbances to the overall heat transfer process, showing up as fluctuations in the recorded inlet temperature [35]. Additionally, the temperature TB was slightly higher than that of TA, and fluctuations occurred during the investigation. From the observation, it can be seen that TC, TD, and TE were slightly different. At 4200s, these temperatures were approximately 27°C. On the other hand, similar fluctuations are observed in TC, TD, and TE as well. In addition, it is evident that the temperature on the outlet side of the evaporator is directly proportional to the temperature on the inlet side of the evaporator. However, the temperature at the outlet side of the evaporator is observed to be lower than the corresponding temperature at the inlet side. This can be attributed to the phenomenon of evaporative cooling, which is the primary function of the evaporator within the refrigeration cycle. As the refrigerant flows through the evaporator, it absorbs heat from the surrounding environment. This heat transfer process facilitates the phase change of the refrigerant from a liquid to a vapor state [22]. The absorption of heat from the room into the evaporator's inlet side provides the necessary latent heat of vaporization for the refrigerant to undergo this phase transition. Consequently, the refrigerant exiting the evaporator outlet side has a lower temperature compared to the inlet side.

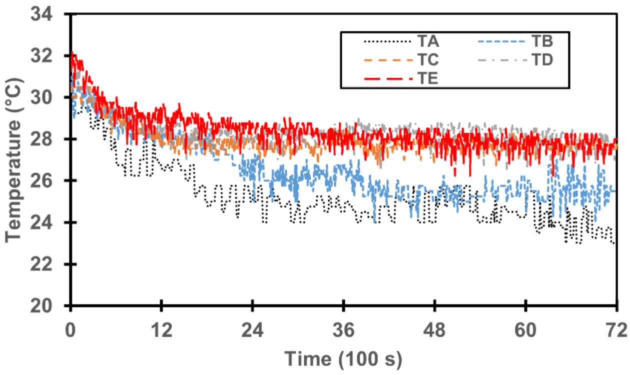

Figure 3. Temperature variation at the evaporator inlet correlated with temperature setpoint

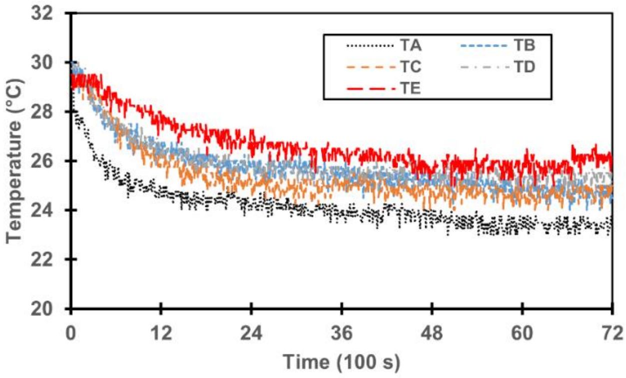

Figure 4. Ambient temperature correlated with temperature setpoint

Figure 4 shows the ambient temperature from each temperature setpoint. It can be seen that the temperature of TA exhibits the lowest value. This minimum temperature can be attained at approximately 24.5°C. The temperatures of TB and TC were found to be nearly equivalent, with minor variations. Both TB and TC sharply decrease to 26°C at the 1110s. Furthermore, the temperature setpoint of TD is slightly higher than that of TB and TC. However, it remains relatively lower compared to the temperature of TE. The highest ambient temperature was observed for TE. It is evident that TE represents the highest temperature setpoint, approximately 20°C. This observation is consistent with the expectation that a higher temperature setpoint would result in higher ambient temperatures within the conditioned space. Generally, the range of ambient temperatures exhibited across all the evaluated conditions falls within the typical comfort temperature range for Indonesia, a tropical country characterized by high humidity levels. The suitability of these temperature ranges for ensuring thermal comfort in such climatic conditions is a crucial consideration in the design and operation of air conditioning and refrigeration systems [36].

3.2 Temperature Differential

Figure 5 shows the temperature differential between the inlet and outlet of the evaporator based on temperature setpoint. From Figure 5(a), it is apparent that the temperature differential initially increases significantly, reaching approximately 10°C around 220s for the temperature setpoint of 16°C. The average temperature differential observed during the investigation was 11.19°C. On the other hand, the average temperature differential for the temperature setpoints of 17°C was observed to be 12.31°C as shown in Figure 5(b). These results are slightly higher compared to the temperature setpoint of 16°C as shown in Figure 5(b). The temperature differential across the evaporator is influenced by several factors, including the cooling load imposed on the system and the prevailing environmental conditions within the conditioned space [37]. These factors can contribute to variations in the heat transfer rates and, consequently, the observed temperature differential. The temperature differential for the temperature setpoint of 18°C can be seen in Figure 5(c). From the analysis, the initial surge in temperature differential was lower compared to both temperature setpoints of 16°C and 17°C. However, the average temperature differential for the temperature setpoint of 18°C was found to be 12.76°C. This result is not significantly different from the temperature setpoint of 17°C. Furthermore, the temperature differential for a temperature setpoint of 19°C is shown in Figure 5(d). It can be seen that the average temperature differential exhibits a value of 12.89°C. This result is notably higher than the previous temperature setpoint. Moreover, the temperature differential for the final temperature setpoint of 20°C is shown in Figure 5(e). Based on the observation, the average temperature differential exhibits a value of 12.13°C. No significant difference was found in the investigation.

Regarding evaporator temperature differential standards, a minimum tolerance value of 8°C is typically employed as a metric to evaluate the effectiveness of the heat transfer process and the cooling capacity of the evaporator component. The observed average temperature differentials for all the investigated temperature setpoints exceed this minimum tolerance value, indicating that the evaporator is operating within acceptable performance parameters. The temperature differential across the evaporator is directly proportional to the heat transfer rate occurring within the component. A higher temperature differential corresponds to a more significant heat transfer from the conditioned space to the refrigerant flowing through the evaporator. Consequently, a larger temperature differential is indicative of a more effective evaporative cooling process and a greater cooling capacity of the evaporator [20]. The range of average temperature differentials observed in this investigation, spanning from 11.19°C to 12.89°C, suggests that the evaporator is effectively absorbing heat from the surrounding environment and facilitating the phase change of the refrigerant from liquid to vapor. This heat transfer process is essential for providing the desired cooling effect within the conditioned space. In addition, the temperature differential across the evaporator is also closely linked to the overall energy efficiency of the air conditioning system. A higher temperature differential implies that the evaporator can achieve the desired cooling effect with a lower mass flow rate of refrigerant, potentially reducing the energy consumption associated with the compressor work and enhancing the system's overall efficiency.

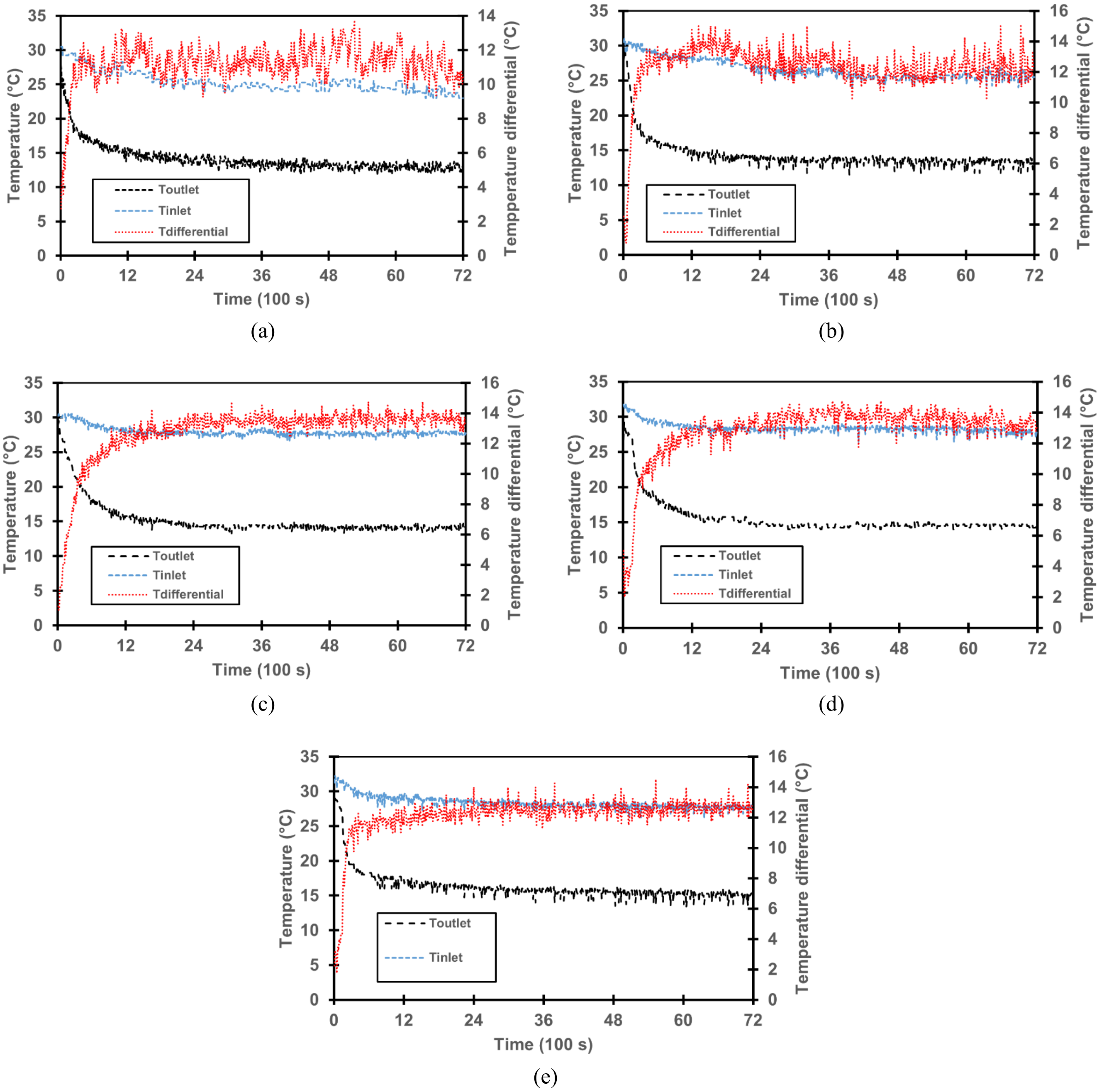

Figure 5. Temperature differential for temperature setpoint of; (a) 16°C; (b) 17°C; (c) 18°C; (d) 19°C; (e) 20°C

3.3 Relative Humidity

Figure 6 shows the relative humidity variation on the evaporator outlet side from each temperature setpoint. The figure shows relative humidity increasing sharply to 90% across all temperature setpoints. This phenomenon can be attributed to the evaporation process, which results in air containing high moisture. When warm air from the room passes through the cold evaporator coil, the air temperature significantly decreases lower than its dew point temperature. This is because water vapor in the air condenses. The evaporation of the refrigerant within the evaporator coils is an endothermic process, meaning that it absorbs latent heat from the surrounding air. This latent heat is required for the phase change of the refrigerant from liquid to vapor. As the refrigerant evaporates, it extracts both sensible heat and latent heat from the air stream. Figure 6 illustrates the RHA reached 94.2% in the 1200s and then remained relatively constant. Moreover, RHA, RHB, and RHC tend to be the same, with minor fluctuations occurring during the investigation. This similarity can be attributed to the comparable evaporation rates and cooling capacities of the evaporator coils at this temperature setpoint. The evaporation process in the evaporator coils absorbs latent heat from the surrounding air, causing the relative humidity to rise [17]. In addition, RHD and RHE were lower, around 89% at 2400s and relatively constant. Based on the observation, the sharp increase in relative humidity is a fundamental characteristic of air conditioning cooling systems, and this phenomenon is required for dehumidification and effective cooling of space.

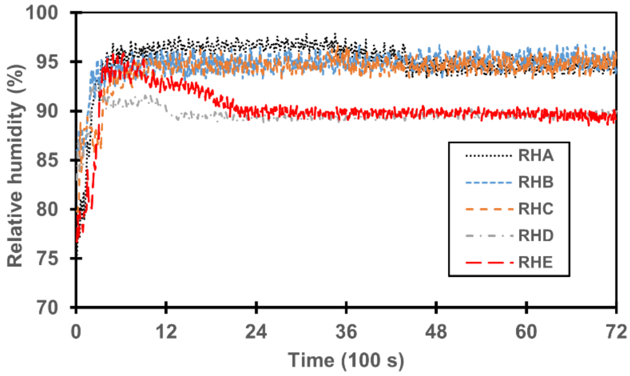

Figure 6. Relative humidity variation at the evaporator outlet correlated with temperature setpoint

Relative humidity variation on the evaporator inlet side from each temperature setpoint can be shown in Figure 7. From Figure 7, all temperature setpoints demonstrated a rapid reduction in relative humidity. This is because the initial moisture content of the air was too high, and the temperature was significantly different between the inlet and outlet evaporator sides. When the air passes over the evaporator coils, the condensation process occurs rapidly, resulting in a significant decrease in relative humidity. From the observation, both RHA and RHB showed a similar trend of reduction to 60% at 2270s and then tended to approach each other. Similar results were found in RHC and RHD. At about 3040s, both RHC and RHD were at 60%. During investigation, the relative humidity was found to be decreasing slowly due to the reduced temperature difference and the decreasing moisture content of the air. The higher the temperature setpoint, the higher the initial relative humidity, as the warmer air held more moisture. Nevertheless, as the air travels through the evaporator, the relative humidity shows a similar final result, which indicates that the air has reached a state of dehumidification [38].

Figure 8 shows the ambient relative humidity from each temperature setpoint. It can be seen that all the variables show a high relative humidity of around 75% at 0s and then a relative decrease. When the air conditioning starts to operate, the relative humidity levels indicate a gradual decrease across all temperature setpoints. RHA was found to be 62.7% at 2400s, 65.1% for RHB and 64.2% for RHC. Furthermore, RHD and RHE show 65% and 65.5% respectively at 2400s. The rate of reduction in relative humidity is higher for lower temperature setpoints. From Figure 8, RHA shows the fastest reduction, while RHE indicates the slowest reduction. At a lower temperature setpoint, the air conditioning system must remove a greater quantity of sensible heat from the air to achieve the desired cooling effect [19]. This process involves the expansion of the refrigerant gas, which absorbs heat from the surrounding air, causing the air temperature to decrease. As the air temperature decreases, its capacity to hold water vapor also decreases, according to the principles of psychrometrics. When the air temperature drops below the dew point temperature, the excess water vapor in the air condenses onto the cooling coils of the air conditioning unit, thereby reducing the moisture content and, consequently, the relative humidity of the air. In addition, the lowest relative humidity can be reached about 58%. After around 3600s, the relative humidity was stabilized and fluctuated around specific levels. The lower temperature setpoint indicated the more effective dehumidification.

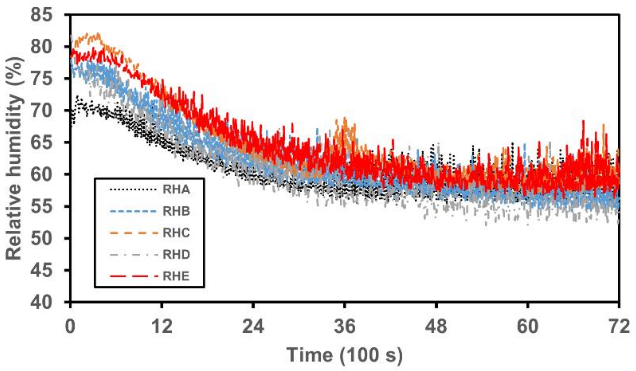

Figure 7. Relative humidity variation at the evaporator inlet correlated with temperature setpoint

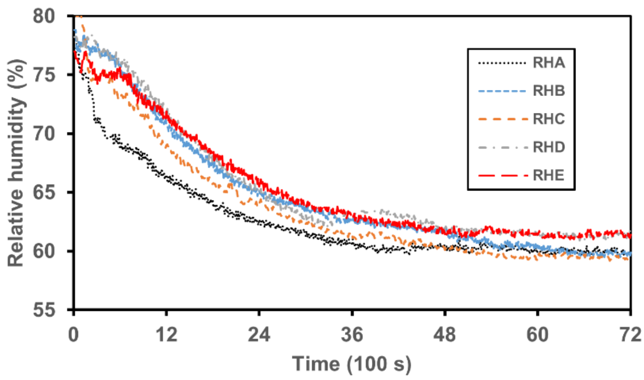

Figure 8. Ambient temperature correlated with temperature setpoint

3.4 Psychrometric Analysis

An online psychrometric chart calculator is used to determine thermodynamic properties, including parameters such as enthalpy, specific volume, humidity ratio, specific heat, and dew point temperature. Table 4 shows the thermodynamic properties of each temperature setpoint. The psychrometric chart cycle for each temperature setpoint is shown in Figure 9. These psychrometric charts are displayed in imperial units. All temperature results have been converted to imperial units to facilitate plotting on the psychrometric charts. The average inlet temperature for the setpoint of 16°C was found to be 25.29°C and 60.89% for the average relative humidity. Subsequently, the average inlet temperature for the setpoint of 17°C was 26.55°C, and the average relative humidity was 62.32%. At setpoint 18°C, the average temperature was 27.94°C and the average relative humidity inlet was 64.8%. The average inlet temperature for the setpoint 19°C was 28.4°C and 60.58% for the relative humidity. At setpoint 20°C, the average inlet temperature and relative humidity was 28.4°C and 64.7% respectively. The average outlet temperature for the 16°C setpoint was found to be 14.09°C, and the average relative humidity was 95.08%. For the 17°C setpoint, the average temperature was 14.23°C, and the average relative humidity was 94.71%. At the 18°C setpoint, the average temperature was 15.18°C, and the average relative humidity was 94.18%. The average outlet temperature for the 19°C setpoint was 15.50°C, and the average relative humidity was 89.65%. For the 20°C setpoint, the average temperature was 16.26°C, and the average relative humidity was 90.16%.

Table 4. Thermodynamic properties of the air

Temperature setpoint (°C)	Relative Humidity (%)	Humidity Ratio (g/kg)	Specific Heat (kJ/kg.K)	Temperature Dew Point (°C)	Enthalpy (kJ/kg)	Specific Volume (m^3/kg)
Inlet 16	60.89	12.340	1.023	17.200	56.862	0.862
Inlet 17	62.32	13.635	1.025	18.762	61.460	0.868
Inlet 18	64.80	15.424	1.027	20.703	67.458	0.874
Inlet 19	60.58	15.424	1.026	20.703	67.458	0.874
Inlet 20	64.70	15.829	1.027	21.113	68.965	0.876
Outlet 16	95.08	9.567	1.018	13.316	38.343	0.826
Outlet 17	94.71	9.618	1.018	13.395	38.614	0.827
Outlet 18	94.18	10.178	1.019	14.253	41.002	0.830
Outlet 19	89.65	89.650	1.018	13.810	40.589	0.831
Outlet 20	90.16	90.160	1.019	14.647	42.786	0.834
Ambient 16	62.69	11.888	1.023	16.631	54.582	0.858
Ambient 17	64.80	13.504	1.024	18.611	60.282	0.865
Ambient 18	63.71	12.915	1.024	17.915	58.318	0.863
Ambient 19	65.46	13.819	1.025	18.972	61.301	0.866
Ambient 20	65.34	14.406	1.025	19.625	63.539	0.869

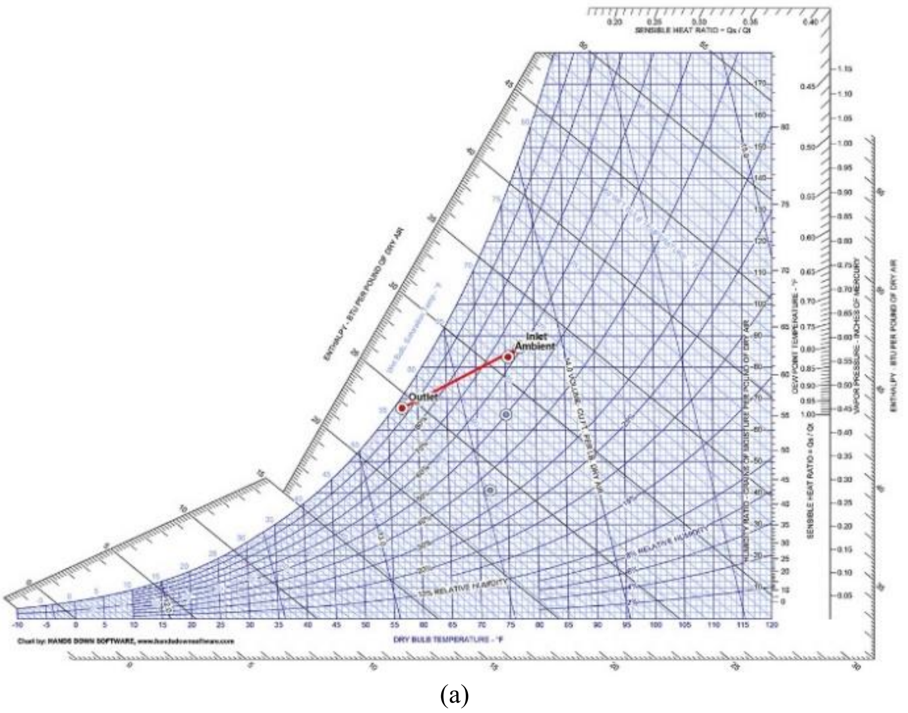

(a)

Figure 9. (a) Psychrometric chart cycle related to a temperature setpoint of 16°C

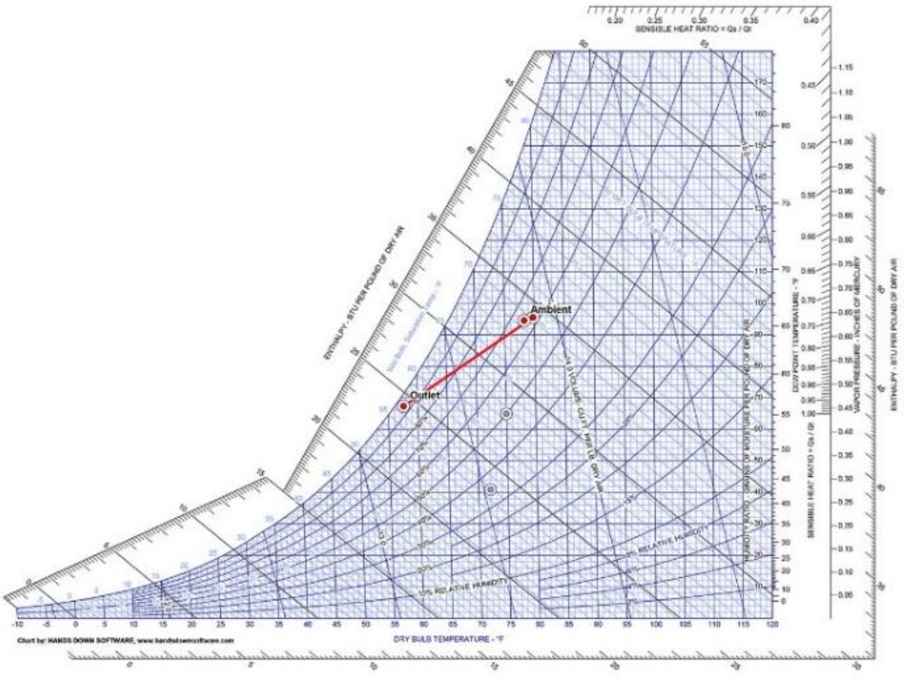

(b)

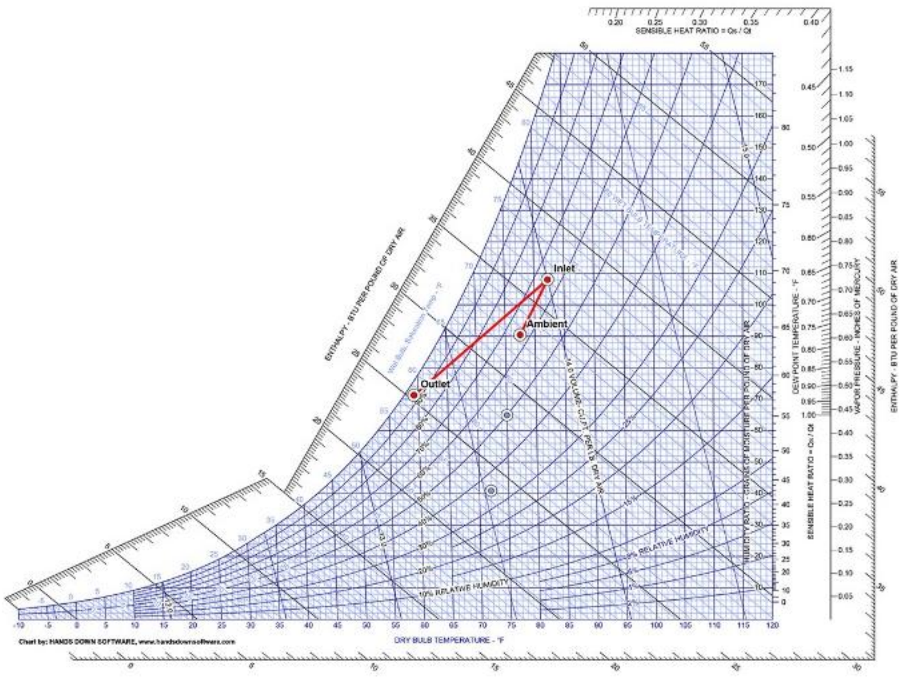

(c)

Figure 9. (cont.) (b) Psychrometric chart cycle related to a temperature setpoint of 17°C; (c) Psychrometric chart cycle related to a temperature setpoint of 18°C

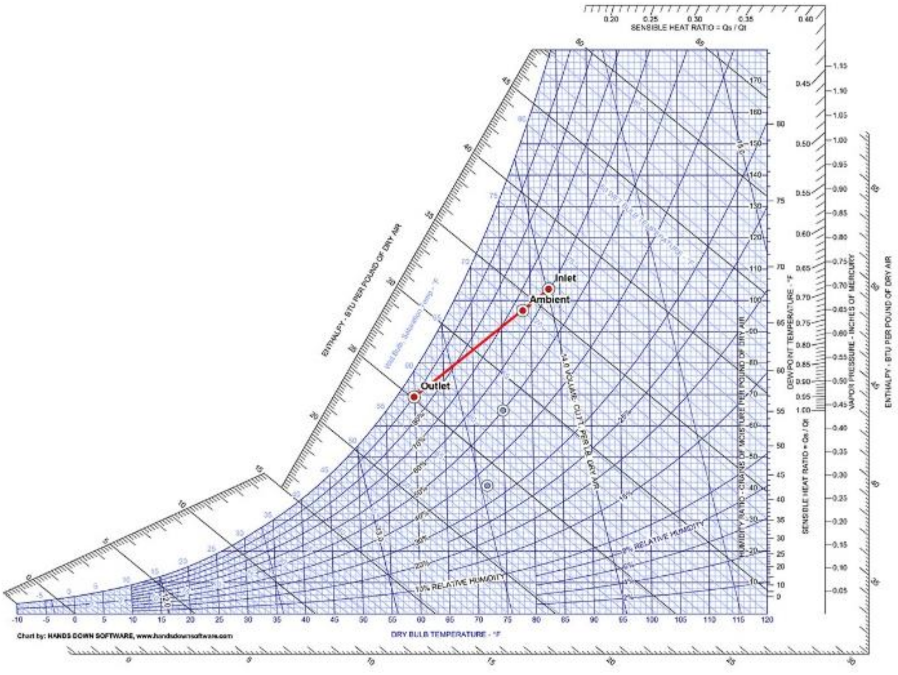

(d)

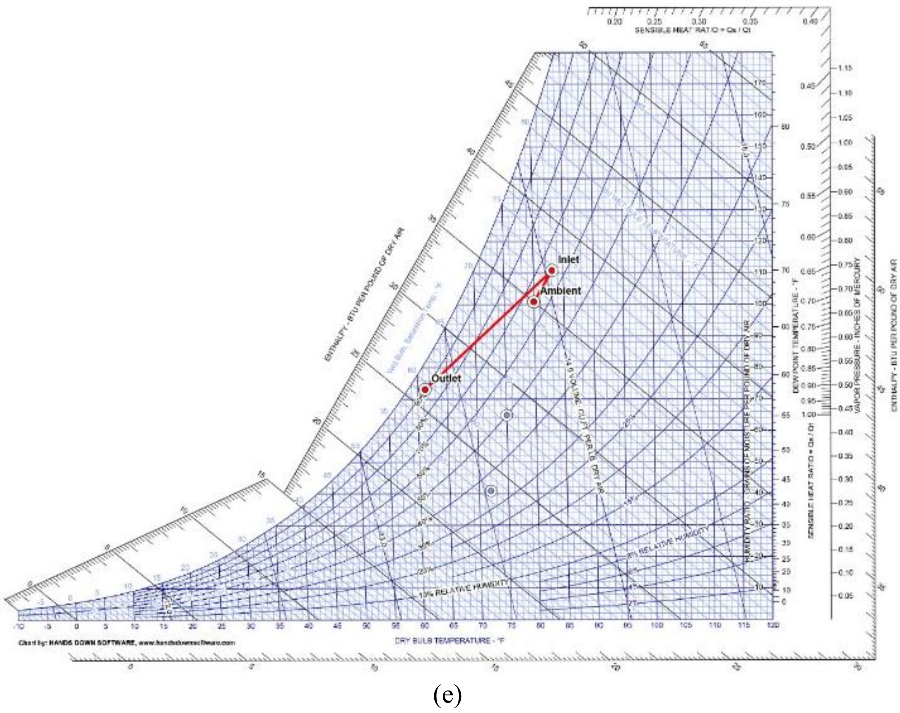

(e)

Figure 9. (cont.) (d) Psychrometric chart cycle related to a temperature setpoint of 19°C; (e) Psychrometric chart cycle related to a temperature setpoint of 20°C

In addition, the average ambient temperature and relative humidity for the setpoint of 16°C were observed to be 24.19°C and 62.69%, respectively. At the temperature setpoint of 17°C, the average ambient temperature and relative humidity were 25.73°C and 64.8%, respectively. The average ambient temperature for the setpoint of 18°C was 25.28°C, and the average relative humidity was 63.71%. At the setpoint of 19°C, the average ambient temperature was 25.94°C, and the average relative humidity was 65.46%. Additionally, the average ambient temperature and relative humidity for the setpoint of 20°C were observed to be 26.66°C and 65.34%, respectively. The properties of air at the evaporator inlet and outlet sides, as well as the ambient conditions for each temperature setpoint, can be seen in Figure 10.

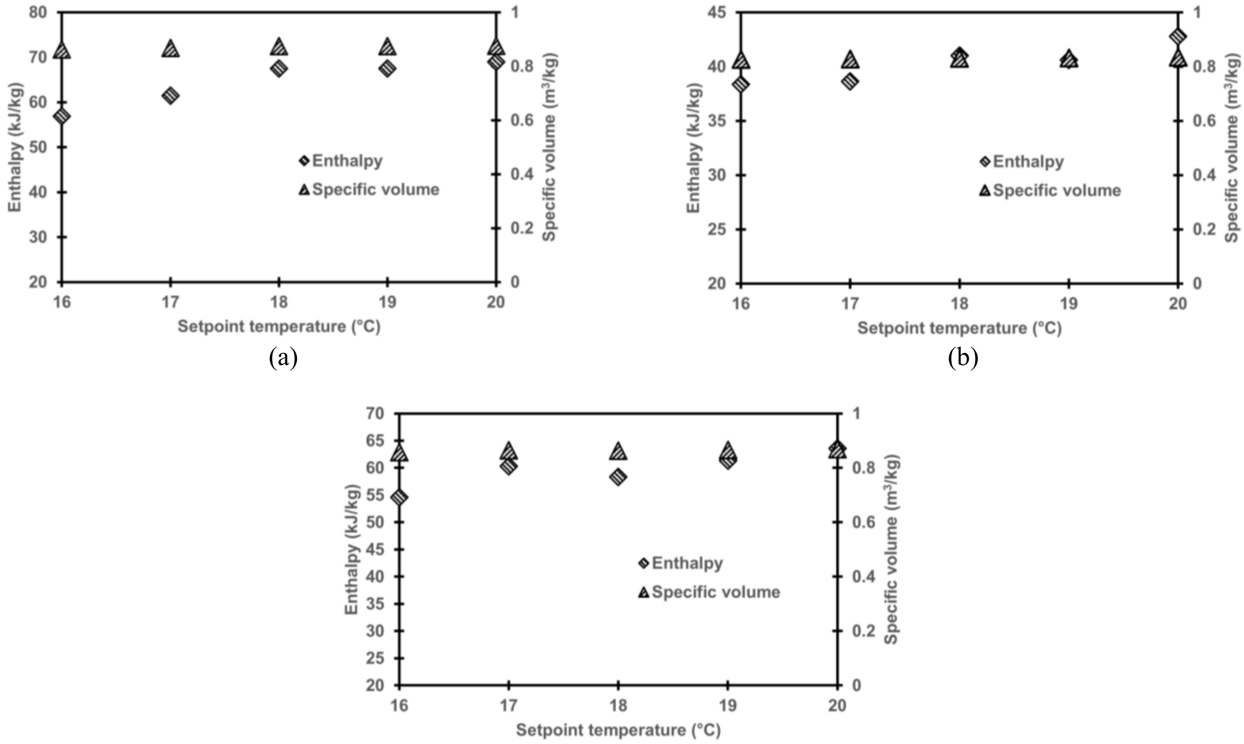

(c)

Figure 10. Air properties at (a) inlet side of the evaporator; (b) outlet side of the evaporator; (c) ambient conditions

3.5 Electrical Characteristic

Figure 11(a) shows the voltage from each temperature setpoint. The fluctuations were found in the voltage levels as the air conditioning cooling system begins with frequency and varying degrees of intensity depending on the temperature setpoint. These fluctuations are caused by the cooling load on the air conditioning device, which maintains the indoor temperature and relative humidity. From Figure 11(a), it can be seen that the VA and VB show more frequent and larger voltage fluctuations from the baseline level. This behavior is attributable to the increased cooling load placed on the air conditioning system at these lower temperature setpoints, requiring more frequent compressor cycling to remove heat from the indoor environment. In addition, some of the voltage fluctuations evident in the profiles likely correspond to the intermittent operation of auxiliary components within the air conditioning unit. These include fans used to circulate air over the evaporator and condenser coils, as well as defrost cycles implemented to prevent ice buildup on the evaporator during periods of high humidity [39].

Figure 11(b) shows the electric current from each temperature setpoint. The sharp increase was found in current across all the temperature setpoints due to the initial current required to operate the compressor and supplementary components of the air conditioning. During the initial phase, observed at approximately 100s, the current reaches a peak value of 1.4A for all temperature setpoints. This surge in current is attributable to the high inrush current demanded by the air conditioning compressor and auxiliary components, such as fans and control circuitry, during the startup sequence. Furthermore, the current profiles exhibit a gradual increase, eventually stabilizing at approximately 2.30A around 400s. This sustained current level corresponds to the steady-state operating condition of the air conditioning system, where the compressor and associated components are actively engaged in maintaining the desired indoor temperature and humidity levels. The lower temperature setpoint generally exhibits higher steady-state current demands compared to the higher temperature setpoint. This behavior is expected, as lower temperature setpoint impose a greater cooling load on the air conditioning unit, necessitating increased energy consumption to remove the additional heat from the indoor environment. Despite the overall stability of the current profiles during steady-state operation, minor fluctuations are observed across all temperature setpoints. These fluctuations can be attributed to variations in room conditions [40], such as changes in ambient temperature, humidity levels, or occupancy patterns, which influence the cooling load and subsequently impact the energy consumption of the air conditioning system.

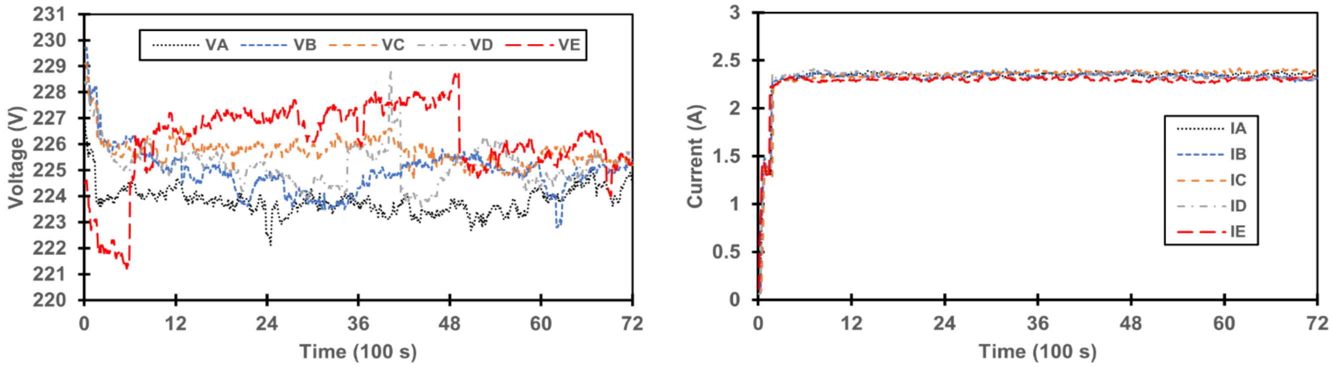

(a) (b)

Figure 11. Temperature setpoint correlation with; (a) voltage variation; (b) electric current variation

Figure 12 shows the power consumption from each temperature setpoint. At approximately 600s, a significant increase in power consumption is observed, reaching a peak value of approximately 400w for all temperature setpoints. This surge in power demand is directly attributed to the increased workload placed on the compressor during the initial cooling phase, as it expends substantial energy to remove heat from the indoor environment and achieve the desired temperature setpoint. Subsequent to this initial transient period, the power consumption profiles exhibit minor fluctuations around a sustained level, which varies with the respective temperature setpoint. These fluctuations are indicative of the dynamic nature of the cooling process, where the air conditioning unit modulates its power consumption in response to changes in the thermal load, ambient conditions, and other external factors affecting the cooling demand. From Figure 12, the direct proportionality between the power consumption and the electric current drawn by the air conditioning unit can be observed. As the current increases, a corresponding rise in power consumption is observed, reflecting the fundamental relationship between electrical power, voltage, and current in accordance with Ohm's law [41]. Furthermore, an inverse relationship between the temperature setpoint and the steady-state power consumption levels can be seen. As the temperature setpoint increases from PA to PE, the power consumption decreases accordingly. This behavior is expected, as higher temperature setpoint require a reduced cooling effort from the air conditioning unit, thereby lowering the energy demand and associated power consumption [42]. In addition, the power consumption of an air conditioning system is influenced by various factors beyond the temperature setpoint. These include the thermal load imposed by external conditions, such as ambient temperature, solar radiation, and occupancy levels, as well as the efficiency and performance characteristics of the air conditioning unit itself.

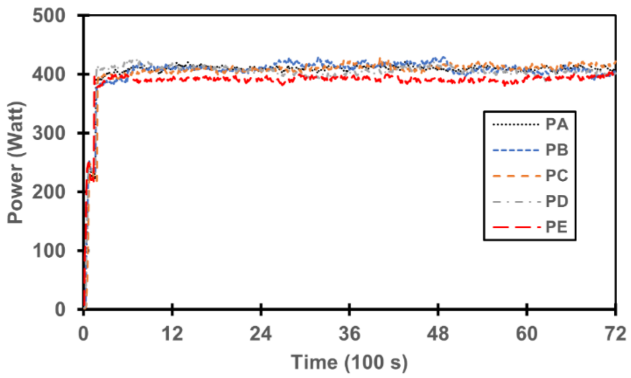

Figure 12. Power consumption variation correlated with temperature setpoint

3.6 Energy Efficiency Ratio

Figure 13 shows the thermodynamic properties of the energy efficiency ratio (EER) from each temperature setpoint. It can be seen that the EER gradually increases with an increase in temperature. At temperature setpoint 16°C, the observed EER was 10.25 and 10.51 for temperature setpoint 17°C. Both temperature setpoints, 16°C and 17°C, almost show no significant difference. The air conditioning cooling system works harder to maintain the desired temperature difference between indoor and outdoor environments. This phenomenon causes a lower EER value. Subsequently, temperature setpoints 18°C and 19°C show a slight increase compared to temperature setpoints 16°C and 17°C, which were 11.74 and 12.24 respectively. This improvement in efficiency can be explained by the reduced temperature difference between the indoor and outdoor environments, which results in lower cooling demand and, consequently, a more efficient operation of the air conditioning unit [43]. However, the most significant enhancement in EER is observed at the highest temperature setpoint of 20°C, where the EER reaches a value of 13.87. This substantial increase in efficiency can be attributed to the further reduction in the cooling load as the temperature difference between the indoor and outdoor environments becomes smaller. At these higher temperature setpoints, the air conditioning system can operate more efficiently, as the compressor and associated components are subjected to lower thermal stresses and energy demands.

Moreover, all the temperature setpoints investigated in this study exhibit EER values within the range of 8 to 15, which is generally considered an efficient operating range for residential air conditioning systems [27]. This indicates that the air conditioning unit employed in this study can be categorized as an efficient cooling system capable of providing effective cooling while minimizing energy consumption. In addition, the relationship between temperature setpoint and EER can be explained by the fundamental principles of thermodynamics and the vapor-compression refrigeration cycle employed in air conditioning systems. As the temperature setpoint increases, the energy required to achieve the desired cooling effect decreases, leading to a higher EER. This is because the compressor needs to work less to maintain a smaller temperature differential, resulting in lower energy consumption while still providing adequate cooling capacity.

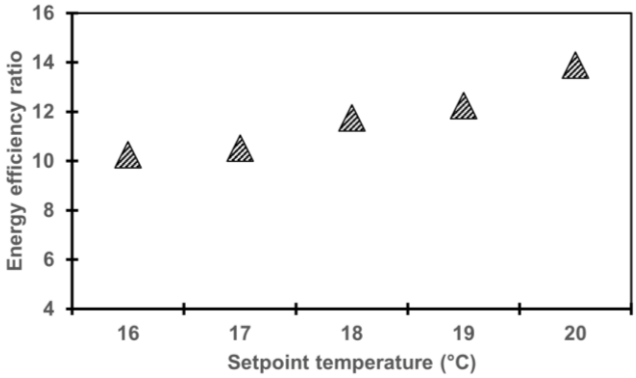

Figure 13. Energy efficiency ratio correlated with temperature setpoint

4. CONCLUSIONS

The energy efficiency ratio (EER) of split inverter air conditioning depends on variations in temperature setpoint, which has been investigated in this study. The highest EER value was found at a temperature setpoint of 20°C, which is 13.87. The higher the temperature setpoint, the higher the EER value of split inverter air conditioning. All temperature setpoints ranging from 16°C to 20°C yielded EER values within the range of 8 to 15, which is considered efficient for residential air conditioning applications. The split inverter air conditioning system employed in this study was deemed efficient for residential use. This finding highlights the suitability of split inverter air conditioning systems for residential cooling purposes, as they can maintain desirable indoor temperatures while operating within the bounds of energy efficiency. In addition, the temperature differential between the inlet and outlet sides of the evaporator has a good differential for the standard differential tolerance of air conditioning. The investigation revealed an average temperature differential of 11.19°C to 12.89°C across all temperature setpoints, indicating the evaporator's efficacy in absorbing heat for the liquid refrigerant to undergo vapor evaporation. The use of microcontroller technology in this study facilitated the real-time recording of each investigation parameter, thereby enhancing the experimental process's efficiency, sophistication, and reliability. Moreover, microcontrollers are programmable, allowing customized algorithms and data processing routines to be implemented. This capability enabled real-time data processing, analysis, and visualization, eliminating the need for time-consuming post-processing steps and providing immediate feedback on the system's behavior. By leveraging the capabilities of microcontroller technology, this study established an automated and streamlined approach to cooling system investigations. The real-time data acquisition, processing, and analysis capabilities provided by microcontrollers not only enhanced the efficiency of the experimental process but also minimized the potential for human error, improving the overall reliability and reproducibility of the results.

ACKNOWLEDGEMENT

The authors would like to express gratitude to the Department of Mechanical Engineering at Bali State Polytechnic and the Refrigeration and Air Conditioning Laboratory for unwavering support in facilitating this research project. The authors acknowledge the financial assistance provided by P3M of Bali State Polytechnic, Indonesia. The resources and support from this department significantly contributed to the success of this research. The authors sincerely thank the department for its invaluable backing throughout this endeavor.

CONFLICT OF INTEREST

The authors affirm that there are no conflicts of interest associated with this research.

AUTHORS CONTRIBUTION

I Gede Artha Negara: Conceptualization, supervision, methodology, validation, writing – review & editing

I Wayan Temaja: Data Acquisition, Software Implementation (ATmega 2560), Data Analysis, Technical Support

Luh Putu Ike Midiani: psychrometric tool development, psychrometric analysis, experimental methodology

I Dewa Made Cipta Santosa: Thermodynamic performance analysis, writing – data analysis

I Gusti Agung Bagus Wirajati: Energy efficiency interpretation, practical application, writing – discussion
Made Ery Arsana: Literature review, hypothesis formulation, writing – review & editing

REFERENCES

[1] M. Dai, H. Li, X. Li, and S. Wang, "Reconfigurable supply-based feedback control for enhanced energy flexibility of air-conditioning systems facilitating grid-interactive buildings," *Advances in Applied Energy*, vol. 14, p. 100176, 2024.

[2] T. Randazzo, F. Pavanello, and E. De Cian, "Adaptation to climate change: Air-conditioning and the role of remittances," *Journal of Environmental Economics and Management*, vol. 120, p. 102818, 2023.

[3] I. M. Rasta and I. N. Suamir, "The role of vegetable oil in water based phase change materials for medium temperature refrigeration," *Journal of Energy Storage*, vol. 15, pp. 368–378, 2018.

[4] H. Zhu, S. Hu, G. Wang, L. Han, M. Jing, and X. Zhao, "Full-scale numerical simulation and experimental validation of the thermal environment under the heating mode in an air-conditioned room," *Case Studies in Thermal Engineering*, vol. 51, p. 103548, 2023.

[5] M. H. Alhamdo, M. A. Theeb, and J. J. Abdulhameed, "Performance Improvement of an Air-Conditioning System During Refrigerant Evaporation," *Journal of Engineering and Sustainable Development*, vol. 2018, no. 6, pp. 101–113, 2018.

[6] Á. Andrade, Á. Restrepo, and J. E. Tibaquirá, "EER or Fcsp: A performance analysis of fixed and variable air conditioning at different cooling thermal conditions," *Energy Reports*, vol. 7, pp. 537–545, 2021.

[7] S. Sheng, T. Yamanaka, T. Kobayashi, N. Choi, and S. Yodono, "Draft-free air conditioning through split membrane ceiling system_ An exploratory study," *Indoor Environments*, vol. 1, no. 2, p. 100017, 2024.

[8] D. Lee and S. T. Lee, "Artificial intelligence enabled energy-efficient heating, ventilation and air conditioning system: Design, analysis and necessary hardware upgrades," *Applied Thermal Engineering*, vol. 235, p. 121253, 2023.

[9] S. Alshammari, S. T. Kadam, and Z. Yu, "Assessment of single rotor expander-compressor device in combined organic Rankine cycle (ORC) and vapor compression refrigeration cycle (VCR)," *Energy*, vol. 282, p.128763, 2023.

[10] S. A. Bhat, U. Sajjad, I. Hussain, W. M. Yan, H. M. U. Raza, H. M. Ali, M. Sultan, H. Omar, M. W. Azam, F. Bozzoli, and N. F. Huang, "Experiments and modeling on thermal performance evaluation of standalone and M-cycle based desiccant air-conditioning systems," *Energy Reports*, vol. 11, pp. 1445–1454, 2024.

[11] C. Liang, F. Zha, and X. Li, "Low-grade energy-bus air conditioning system using energy efficient three-fluid heat exchange terminals," *Next Energy*, vol. 3, p. 100098, 2024.

[12] M. H. Alhamdo, M. A. Theeb, and J. J. Abdulhameed, "Using Evaporative Cooling Methods for Improving Performance of an Air-cooled Condenser," *Universal Journal of Mechanical Engineering*, vol. 3, no. 3, pp. 94–106, 2015.

[13] M. Schweizer, M. Stöckl, R. Tutunaru, and U. Holzhammer, "Influence of heating, air conditioning and vehicle automation on the energy and power demand of electromobility," *Energy Conversion and Management: X*, vol. 20, 2023.

[14] T. Yamamoto, A. Ozaki, K. Aratsu, and R. Fukui, "Energy simulation and CFD coupled analysis for the optimal operation of combined convection and radiant air conditioning considering dehumidification," *Heliyon*, vol. 9, no. 7, p. e18092, 2023.

[15] H. Omar, U. Sajjad, I. Hussain, S. A. Bhat, M. Sultan, H. M. Ali, K. Hamid, and W. Yan, "Influence of the process and regeneration air conditions on the thermal performance of various desiccant air-conditioning systems," *Energy Conversion and Management: X*, vol. 22, p. 100582, 2024.

[16] D. Saad and M. S. Kassim, "Effect of Baffles Geometry on Heat Transfer Enhancement inside Corrugated Duct," *International Journal of Mechanical Engineering and Technology (IJMET)*, vol. 10, no. 03, pp. 555–566, 2019.

[17] H. Zhang, C. Fan, T. Xiong, G. Liu, and G. Yan, "Improving performance of air conditioning system by using variable-circuit heat exchanger: Based on the Chinese APF standard," *Case Studies in Thermal Engineering*, vol. 50, p. 103422, 2023.

[18] J. Li and B. Li, "Scenario analysis of hydrofluorocarbons consumption and emission reduction in China's mobile air-conditioning sector," *Energy Reports*, vol. 11, pp. 3171–3185, 2024.

[19] A. Andrade, J. Zapata-Mina, and A. Restrepo, "Exergy and environmental assessment of R-290 as a substitute of R-410A of room air conditioner variable type based on LCCP and TEWI approaches," *Results in Engineering*, vol. 21, p. 101806, 2023.

[20] A. Esmaeel, A. Rahimnejad, and S. A. Gadsden, "Home energy management system for smart buildings with inverter-based air conditioning system," *International Journal of Electrical Power and Energy Systems*, vol. 133, p. 107230, 2021.

[21] L. Zhu, J. Hong, S. Yang, Z. Hu, Y. Shao, and C. Wu, "Online modeling of virtual energy storage for inverter air conditioning clusters in CDL-based demand response," *Energy Reports*, vol. 9, no. 2023, pp. 2024–2034, 2024.

[22] S. Liu, W. Ge, and X. Meng, "Influence of the shading nets on indoor thermal environment and air-conditioning energy consumption in lightweight buildings," *Energy Reports*, vol. 11, pp. 4515–4521, 2024.

[23] Y. Ding and J. Fournier, "Modeling and analysis of inverter air conditioners for primary 15th analysis Modeling and air conditioners for primary frequency control considering signal delays and detection errors frequency control considering signal delays and detection errors Assess," *Energy Procedia*, vol. 158, pp. 4003–4010, 2019.

[24] R. Conte, M. Azzolin, S. Bernardinello, and D. Del Col, "Experimental investigation of large scroll compressors working with six low-GWP refrigerants," *Thermal Science and Engineering Progress*, vol. 44, p. 102043, 2023.

[25] J. Bai, H. Fan, S. Cui, L. Wang, S. He, M. Chen, and H. Zheng, "Experimental study of phase change heat dissipation system based on hydrogen fuel cell," *Case Studies in Thermal Engineering*, vol. 59, p. 104495, 2024.

[26] F. Guo, Z. Chen, and F. Xiao, "Fault detection and diagnosis of electric bus air conditioning systems incorporating domain knowledge and probabilistic artificial intelligence," *Energy and AI*, vol. 16, p. 100364, 2024.

[27] W. Watcharajinda, A. Asanakham, T. Deethayat, and T. Kiatsiriroat, "Performance study of open pond as heat sink of water-cooled air conditioner," *Case Studies in Thermal Engineering*, vol. 25, p. 100988, 2021.

[28] A. S. Kvalsund and D. Winkler, "Development of an Arduino-based , open-control interface for hardware in the loop applications," *HardwareX*, vol. 16, p. e00488, 2023.

[29] B. Nast, A. Reiz, and K. Sandkuhl, "Iot-based diagnostic assistance for energy optimization of air conditioning facilities," *Procedia Computer Science*, vol. 219, pp. 416–421, 2023.

[30] A. Abolore, D. Olurotimi, O. Edward, H. Olajumoke, and F. Nihinlola, "Arduino microcontroller based real-time monitoring of haemodialysis process for patients with kidney disease," *e-Prime - Advances in Electrical Engineering, Electronics and Energy*, vol. 7, p. 100403, 2024.

[31] K. Confidence, L. Bokopane, and K. Kusakana, "Real-time power dispatch in a standalone hybrid multisource distributed energy system using an Arduino board," *Energy Reports*, vol. 7, pp. 479–486, 2021.

[32] J. Ham, Y. Shin, M. Lee, and H. Cho, "Investigation of performance and energy cost of automobile air-conditioner using alternative refrigerants based on thermal comfort using various cooling seats," *Results in Engineering*, vol. 20, p. 101541, 2023.

[33] P. Sphicas and A. Pesyridis, "Investigation of the temporal behavior of desiccant disk for use in dehumidifiers and air conditioners," *Results in Engineering*, vol. 21, p. 101801, 2024.

[34] J. J. Abdulhameed, M. S. Kassim, and M. S. Kadhim, "Experimental investigation of a condenser air humidity effect on superheated degree of compressor," *Journal of Mechanical Engineering Research and Developments*, vol. 44, no. 5, pp. 167–176, 2021.

[35] A. Y. Sulaiman, G. I. Obasi, R. Chang, H. S. Moghaieb, J. D. Mondol, M. Smyth, B. Kamkari, and N. J. Hewitt, "A solar powered off-grid air conditioning system with natural refrigerant for residential buildings: A theoretical and experimental evaluation," *Cleaner Energy Systems*, vol. 5, p. 100077, 2023.

[36] G. K. Murugesan, C. Murugesan, and S. Tamilkolundu, "Assessment of performance and sustainability of waste heat dryer coupled with air conditioner unit during drying of banana slices," *Case Studies in Thermal Engineering*, vol. 59, p. 104506, 2024.

[37] M. Marwan, ST. N. Jabir, H. Hamdani, P. Purwito, A. Aksan, M. Thahir, Ruslan L, S. Sonong, M. Latief, and A. Pangkung, "Temperature Control Strategy to Mitigate Electrical Energy Cost for Air Conditioning," *e-Prime - Advances in Electrical Engineering, Electronics and Energy*, vol. 7, p. 100410, 2024.

[38] C. Chen, H. Yang, X. Li, L. Chen, and M. Shi, "Optimization of solar and heat pump complementary powered desiccant air conditioning system," *Journal of Building Engineering*, vol. 87, p. 109084, 2024.

[39] P. Zi, P. Luo, C. Wang, Q. Wang, B. Zhao, J. Hao, and T. Lan, "Modeling method of variable frequency air conditioning load," *Energy Reports*, vol. 9, pp. 1011–1017, 2023.

[40] F. Guo, Z. Chen, and F. Xiao, "Fault detection and diagnosis of electric bus air conditioning systems incorporating domain knowledge and probabilistic artificial intelligence," *Energy and AI*, vol. 16, p. 100364, 2024.

[41] A. Venkateshvaran *et al.*, "A novel echocardiographic estimate of pulmonary vascular resistance employing the hydraulic analogy to Ohm ' s law," *IJC Heart & Vasculature*, vol. 42, p. 101121, 2022.

[42] P. L. C. Chua. Y. Takane, C. F. Sheng Ng, K. Oka, Y. Honda, Y. Kim, and M. Hashizume, "Net impact of air conditioning on heat-related mortality in Japanese cities," *Environment International*, vol. 181, p. 108310, 2023.

[43] K. Z. Zhao and Z. Y. Su, "Experimental study on refrigeration system performance of pure electric refrigerator car based on medium pressure air supply," *e-Prime - Advances in Electrical Engineering, Electronics and Energy*, vol. 7, p. 100399, 2024.